CHAOTIC ATTRACTORS AND EVOLVING PLANAR SYMMETRY

JEFFREY P. DUMONT
Lafayette College, Box 7756, Easton PA 18042, U.S.A.
e-mail: dumontj@lafayette.edu

FLYNN J. HEISS
57 Main Street, Geneseo NY 14454, U.S.A.
e-mail: fjh1@uno.cc.geneseo.edu

KEVIN C. JONES
3329 25th Avenue, Moline IL 61265, U.S.A.
e-mail: kjones15@uic.edu

CLIFFORD A. REITER
Department of Mathematics, Lafayette College, Easton PA 18042, U.S.A
e-mail: reiterc@lafcol.lafayette.edu

LISA M. VISLOCKY
Lafayette College, Box 9486, Easton PA 18042, U.S.A.
e-mail: vislockl@lafayette.edu

Abstract—Building upon work which illustrated families of chaotic functions with planar symmetries, we explore evolving attractors from one symmetry type to another. We observe different ways the symmetries evolve and pay attention to those which exhibit degenerate behavior. Visually attractive images with low symmetry can be created in this way.

1. INTRODUCTION

Chaos has been the subject of much recent study. Remarkably, symmetry may appear even in the presence of chaos. Field and Golubitsky [3] have examined families of functions which can be used to generate chaotic attractors with cyclic, dihedral and some of the planar crystallographic symmetries. Carter et al. [1] have illustrated chaotic attractors with symmetries from each of the frieze and planar crystallographic groups. Polar variants [2] of that work and extensions to some point groups in higher dimensions

have also appeared [6,7]. Readers can find illustrations of these symmetries in [1], an introduction in [4], and can use the *International Tables for Crystallography* [5] for further reference.

This paper examines families of functions as we shift the symmetry from one planar type to another. Using a fourier series in one coordinate and a power series in the other, the attractors with frieze symmetry in [1] were generated by function classes with many parameters. The functions for the frieze groups split into two types. One involves the addition of an identity function, which is used for the frieze groups that contain glide reflections; the other type does not. Otherwise, the functions differ by which parameters have to be zero. Our experiments involve gradually shifting the parameters so that initially they have the required zeros for one symmetry, but then they evolve so that they have the zeros required for another symmetry. The situation for the planar crystallographic groups is more complicated, but roughly similar, as we will see.

We observe that sometimes one symmetry occurs only at the initial or terminal endpoint of our evolution and at intermediate times the other symmetry prevails. In other cases the symmetry drops to a lower type at intermediate times. The classical bifurcation diagram for the logistic map illustrates that families of chaotic attractors may exhibit simpler, degenerate, behavior in certain parameter windows. Since we are investigating attractors in higher dimensional space, we see such behavior, but with greater diversity. Moreover, when the symmetry type drops during intermediate times, we find the resulting attractors to be more interesting than those found by direct Monte-Carlo searches. Thus, our experiments illustrate effective techniques for finding visually interesting attractors with low symmetry type.

2. Frieze Groups

We begin by investigating families of chaotic attractors with the symmetries of some frieze groups. Our first example looks at a family of chaotic attractors whose symmetry shifts from the group *pma2* to the group *p1a1*. The symmetry group *p1a1* contains a glide reflection which is a combination of a half-period translation followed by a reflection across the center line parallel to the translation. An example appears in the

final frame of Figure 1. The symmetry group *pma2* also contains a glide reflection but has a reflection perpendicular to the axis of the glide reflection. An example appears in the first frame of Figure 1.

Table I Array Masks for p1a1 and pma2

m_1 : p1a1			m_2 : pma2		
1	0	1	0	0	0
0	1	0	0	1	0
0	1	0	0	0	0
1	0	1	1	0	1
1	0	1	0	0	0
0	1	0	0	1	0
0	1	0	0	1	0
1	0	1	0	0	0
1	0	1	1	0	1
0	1	0	0	0	0

In [1] it was seen that to create a chaotic attractor with *p1a1* symmetry, we can use a function $g_A : \Re^2 \to \Re^2$ of the form

$$g_A\langle x, y\rangle = \langle x, 0\rangle + \langle 1, \cos(x), \cos(2x), \sin(x), \sin(2x)\rangle \bullet A \bullet \langle 1, y, y^2\rangle \bmod \langle 2\pi, \infty\rangle$$

where A is a 5 by 2 by 3 array and1 the symbol $\bullet$ stands for the generalized matrix product which takes dot products of the last axis of its left argument with the first axis of its right argument in all possible ways. In order to obtain the *p1a1* symmetry, we need certain entries of A to be zero. Namely, those positions indicated by a zero in the mask m_1 need to be zero; m_1 appears in Table I. If we let P be a 5 by 2 by 3 array of numbers, then we will denote by $m_1 * P$ the elementwise product which has the required zeros. By elementwise, we mean that each entry in P is multiplied by the corresponding entry in m_1. Thus, the function $g_{m_1 * P}$ will have the symmetries of *p1a1*. Likewise, $g_{m_2 * P}$ will have the symmetries of *pma2*.

Our approach to the creation of these images follows [1]. Once we obtain the correct mask for our symmetry, we create our matrix P as an array of random numbers.

We multiply P by the mask to obtain our matrix of coefficients A, as described above. The resulting function $g_{m_1 * P}$ is a map of the plane with the desired symmetry. We iterate the function many times, ignoring initial iterates to avoid transient behavior. We test the function to make sure it is not periodic, does not give collinear points, and that the Ljapunov exponent is within bounds indicative of chaos and associated with interesting images [8]. In our situation we demand that these conditions hold for several frames of the evolutions we will describe below. Once we find a set of visually pleasing frames, we iterate the functions many more times to create a high-resolution image. Points that are hit with a different frequency are colored differently, and colors that appear less often tend to indicate high frequency regions. We then choose color palettes for each attractor purely by aesthetic considerations. The background color, white, represents areas not hit by the attractor.

In order to evolve from one symmetry type to another, we consider a smooth transition from one mask to the other using $m_\lambda = m_2\lambda + (1-\lambda)m_1$ for $0 \le \lambda \le 1$. Note that when λ=0, the mask is m_1, and when λ=1, the mask is m_2. The values of λ between 0 and 1 give our intermediate steps between the symmetries *p1a1* and *pma2*. Figure 1 shows the attractors generated by $m_\lambda * P$ for λ=0.00, λ=0.25, λ=0.5, λ=0.75, and λ=1.00, respectively; P is given in the Appendix. The first frame of Figure 1 has both vertical mirrors and a glide reflection. As we increase λ, the glide reflections remain but the vertical mirrors disappear. One can verify that this follows from the overlapping zeros in the masks. An animated version of the evolution appearing in Figure 1 can be found on a link from the gallery on the webpage http://www.lafayette.edu/~reiterc. While the animation appears fairly smooth, the change from a round mirrored *pma2* attractor to a sharp *p1a1* is dramatic. Note that some intermediate frames degenerate and are skipped in the animation. This behavior will be discussed further in the next section. The webpage also provides an animation of a family of chaotic attractors whose frieze pattern *pm11* changes to one with frieze pattern *p1m1*. Note that *pm11* is a symmetry group which contains reflections perpendicular to translations while *p1m1* is a group that has a line of reflection parallel to translations. However, here the intermediate steps all have

only translational symmetry. It can be shown that this follows from the non-overlapping nature of the masks. These masks can be found in [1].

3. Planar Crystallographic Groups

Our first illustration of evolution between planar crystallographic groups is between the two symmetry groups *cm* and *cmm*. The group *cm* has a mirror and a glide reflection in only one direction, as seen in the first frame of Figure 2. On the other hand, the group *cmm* contains two perpendicular lines of reflection as well as glide reflections parallel to those mirrors, as seen in the fourth frame of Figure 2. Attractors with symmetries of both of these groups are obtained by using a truncated fourier series extending in orthogonal directions. The same masking technique is used for this family of chaotic attractors as was used for the frieze groups with the exception that A is now a 5 by 2 by 5 array of parameters. Both *cm* and *cmm* use an identity function in x and y as in [1]; but because *cm* and *cmm* both require the same identity function, it is again possible to create a smooth transition from one symmetry mask to the other. Here we use the function $g_A : \Re^2 \to \Re^2$ which is of the form

$$g_A\langle x, y\rangle = \langle x, y\rangle + \langle 1, \cos(x), \cos(2x), \sin(x), \sin(2x)\rangle \bullet A \bullet \langle 1, \cos(y), \cos(2y), \sin(y), \sin(2y)\rangle \bmod \langle 2\pi, 2\pi\rangle$$

Table II gives the masks required to obtain *cm* and *cmm* symmetries.

Table II Array Masks for cm and cmm

cm					cmm				
1	0	1	0	0	0	0	0	0	0
0	0	0	0	1	0	0	0	0	1
0	1	0	0	0	0	0	0	0	0
0	0	0	1	0	0	0	0	1	0
1	0	1	0	0	0	0	0	0	0
0	0	0	0	1	0	0	0	0	1
0	1	0	0	0	0	1	0	0	0
0	0	0	1	0	0	0	0	0	0
1	0	1	0	0	1	0	1	0	0
0	0	0	0	1	0	0	0	0	0

In this evolution we move from a simple to a more complicated symmetry. Thus, as we move closer to *cmm*, we add a reflection perpendicular to the original reflection. The evolving perpendicular mirrors start to become noticeable in the third frame of Figure 2. During the transition, the attractor retains *cm* symmetry, while moving closer and closer to *cmm* symmetry, which is only achieved at the end. Again, this behavior follows from the overlapping nature of the masks. An animation can be found from the previously mentioned webpage.

The next pair of planar crystallographic groups that we consider is *p2* and *pm*. The symmetry group *p2* has orthogonal translations as well as a rotation of 180° and the group *pm* has perpendicular translations and a reflection. Similar to the technique used to create the functions with *cm* and *cmm* symmetry, truncated fourier series are used to produce those with *p2* and *pm* symmetry. However, they do not incorporate the addition of the term $\langle x, y \rangle$. Table III contains the masks required to produce attractors with *p2* and *pm* symmetry.

Table III Array of Masks for p2 and pm

p2					pm				
0	0	0	1	1	1	1	1	0	0
0	0	0	1	1	0	0	0	1	1
0	0	0	1	1	1	1	1	0	0
0	0	0	1	1	0	0	0	1	1
0	0	0	1	1	1	1	1	0	0
0	0	0	1	1	0	0	0	1	1
1	1	1	0	0	1	1	1	0	0
1	1	1	0	0	0	0	0	1	1
1	1	1	0	0	1	1	1	0	0
1	1	1	0	0	0	0	0	1	1

We notice that the family of chaotic attractors associated with this evolution contain intermediate frames with *p1* symmetry, which contains no symmetry except for translations. These *p1* symmetric attractors appear to be more striking visually than those generated with Monte Carlo searches. Thus, our evolution technique illustrates that searching parameter space for a symmetry group near a more complex symmetry group can lead to more dramatic images.

Our illustration of this evolution is found in Figure 3. Note that the fourth frame contains a degenerate chaotic attractor. Degenerate behavior is commonly found among families of chaotic functions. The bifurcation diagram for the classical logistic function $\lambda\, x(1-x)$, shown in Figure 4, illustrates this. The right portion of this diagram contains apparent gaps in the chaotic regime. All of these are regions where the logistic attractor is simpler. Nonetheless, the form of the chaotic attractor on one side appears to persist across the gap. Such gaps appear in our experiments. For example, in Figure 3, the fourth frame shows a degenerate localized curve-like attractor near the high-frequency areas found in frames 3 and 5. The animation corresponding to this figure shows this behavior as a temporal gap, and moreover, the forms of the images within this gap

change from curve-like, as seen in the figure, to isolated periodic attractors. Since these evolutions are one embedding dimension above the logistic diagram, it is not surprising that these gaps are more diverse. While we highlight the degenerate images found in this family of attractors, we suppress them in the other animations for aesthetic purposes.

Our final illustration of evolution of symmetry groups involves three crystallographic groups containing third turns. These three groups are *p3*, in which none of the third turns contain mirrors; *p31m*, which contains mirrors along some of the third turns; and *p3m1*, in which mirrors are found at every center of rotation. As in [1], we use the symmetry $\sigma_x(x,y) = (x,-y)$ to generate *p31m*; the symmetry $\sigma_y(x,y) = (-x,y)$ is used to generate *p3m1*. To create the family that shifts between these two symmetries, we use the function

$$\sigma_\lambda(x,y) = \left((\sin\pi\lambda + \cos\pi\lambda)x, (\sin\pi\lambda - \cos\pi\lambda)y\right),$$

where λ moves from 0 to 1. In general, as symmetry evolves from *p31m* to *p3m1* there is no symmetry other than the translations. However, we come to a point where *p3* symmetry appears since $\sigma_{1/2}(x,y) = (x,y)$ is the identity function. Figure 5 presents an example of this evolution showing λ=0.00, λ=0.31, λ=0.50, λ=1.00. An animation exhibiting this behavior can be found from the previously mentioned webpage. In addition to the evolution from the frieze group *pm11* to *p1m1* found in this link, there are other animations not discussed in this paper, including evolutions from the crystallographic groups *pgg* to *cm*, and *pgg* to *cmm*.

Acknowledgment – This work was supported in part by DMS-9805507.

REFERENCES

[1] Carter, N. , Eagles, R., Grimes, S., Hahn, A. and Reiter, C. Chaotic Attractors with Discrete Planar Symmetries. *Chaos Solitons & Fractals*, to appear.

[2] Carter, N., Grimes, S., Reiter, C. Frieze and Wallpaper Chaotic Attractors with a Polar Spin. *Computers & Graphics,* to appear.

[3] Field, M. and Golubitsky, M. *Symmetry in Chaos*. Oxford University Press, New York, 1992.

[4] Grünbaum, B. and Shephard, G. C. *Tilings and Patterns*. W.H. Freeman and Company, New York, 1987.

[5] Hahn, T., Editor. *International Tables for Crystallography, Volume A*. Kluwer Academic Publishers, Boston, 1996.

[6] Reiter, C.A. Chaotic Attractors With the Symmetry of a Tetrahedron. *Computers & Graphics*, 1997, **21**, 841-848.

[7] Reiter, C.A. Attractors with the Symmetry of the n-Cube. *Experimental Mathematics*, 1996, **20**, 327-336.

[8] Sprott, J.C. Automatic Generation of Strange Attractors, *Computers & Graphics,* 1993, **17**, 325-332.

APPENDIX

Parameters used for Figure 1:

```
_0.518925  0.431771  0.774487
 0.799078 0.0989788 _0.463648

_0.532977   0.25242   0.43118
 0.838754  0.946274 0.0303457

0.0208725  0.803783 _0.813807
 0.350003  0.503396  0.573136

 0.705091  0.463458 _0.668884
0.0599967  0.364246 _0.111526

_0.416306 _0.860983 _0.537901
_0.505831  0.502622 _0.430047
```

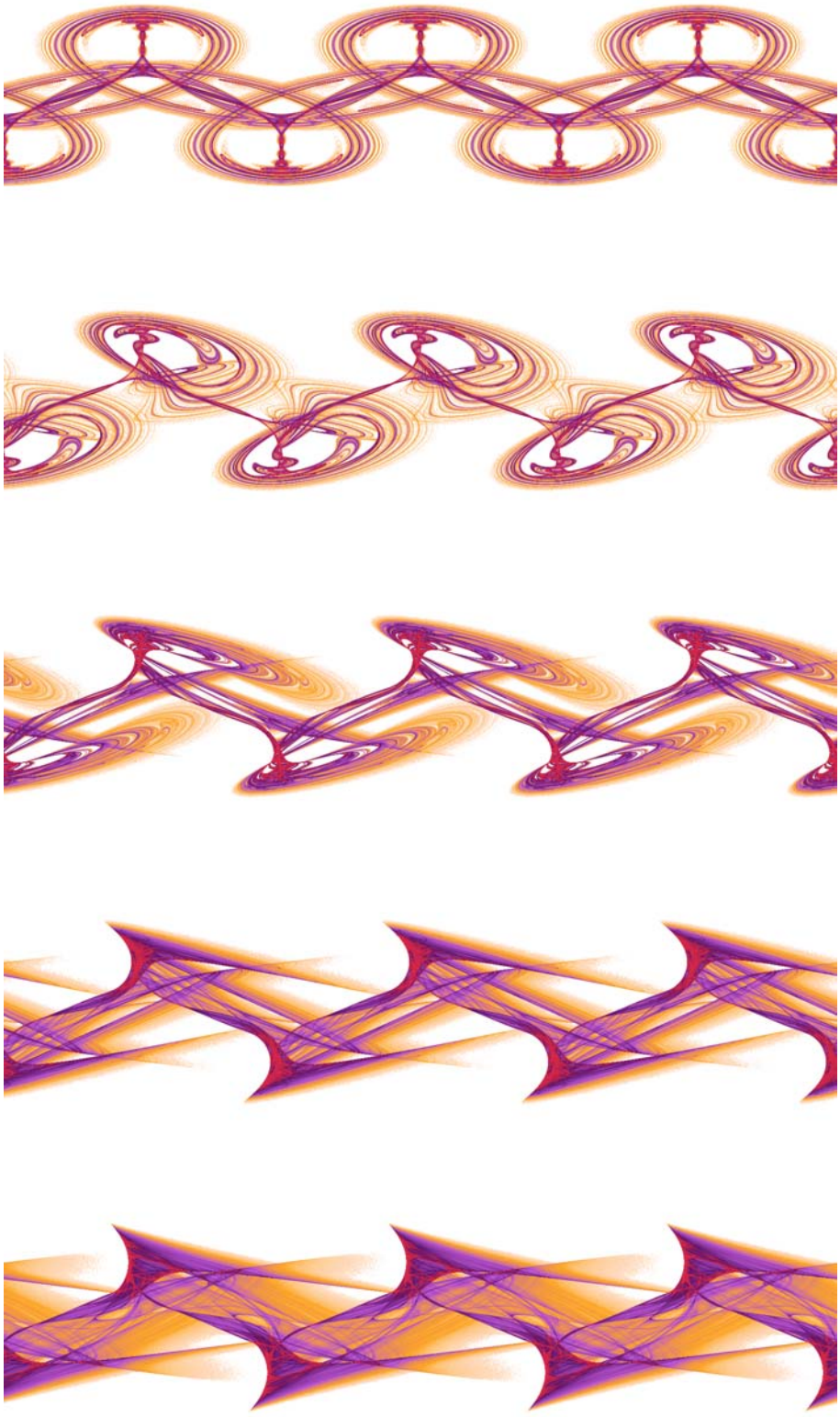

Fig. 1. A family of chaotic attractors evolving from *pma2* to *p1a1* symmetry.

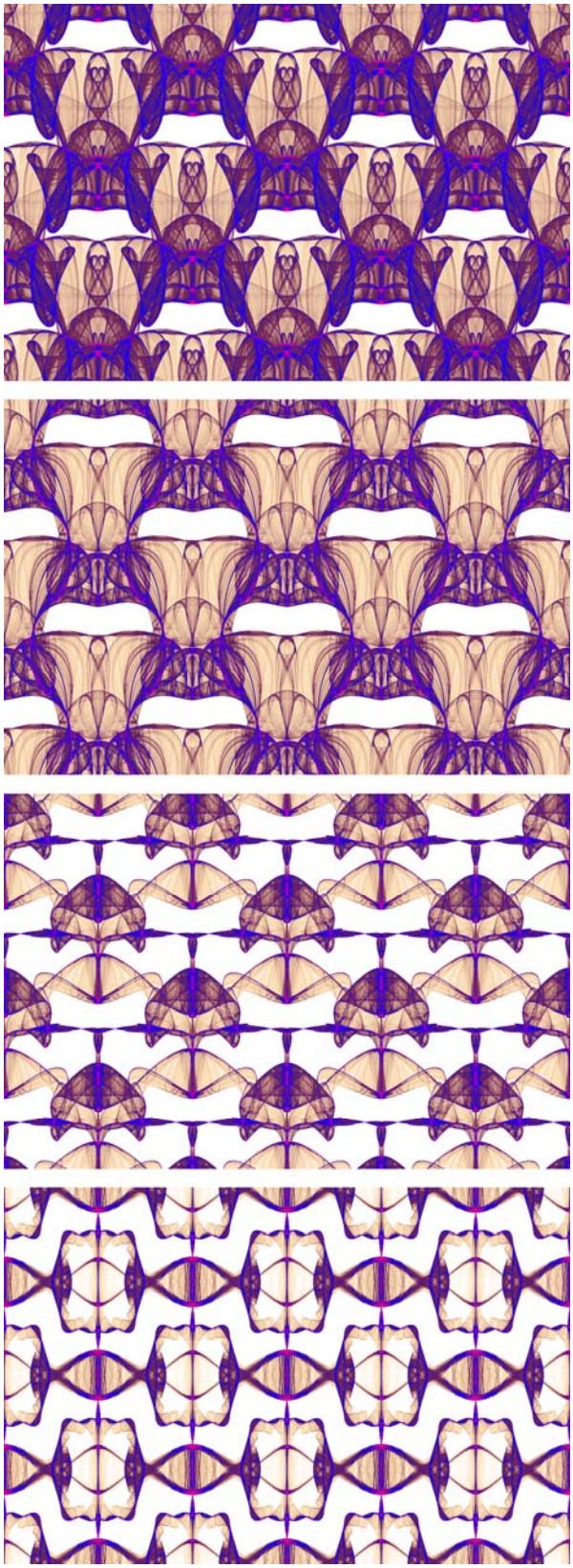

Fig. 2. A family of chaotic attractors evolving from *cm* to *cmm* crystallographic symmetry.

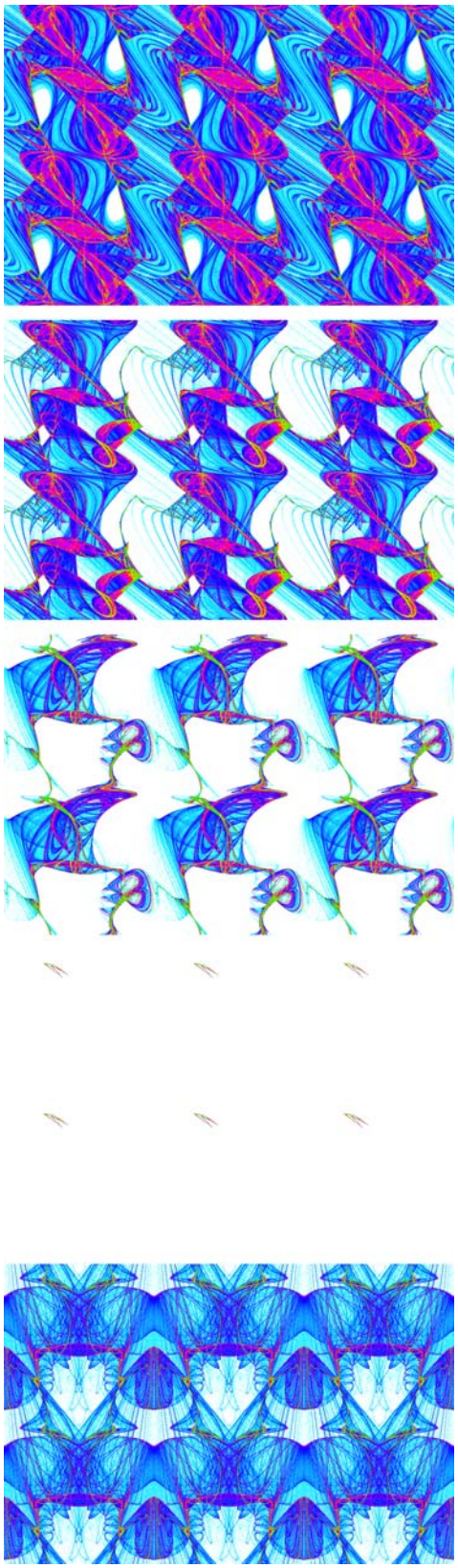

Fig. 3. A family of chaotic attractors evolving from *p2* to *pm* crystallographic symmetry.

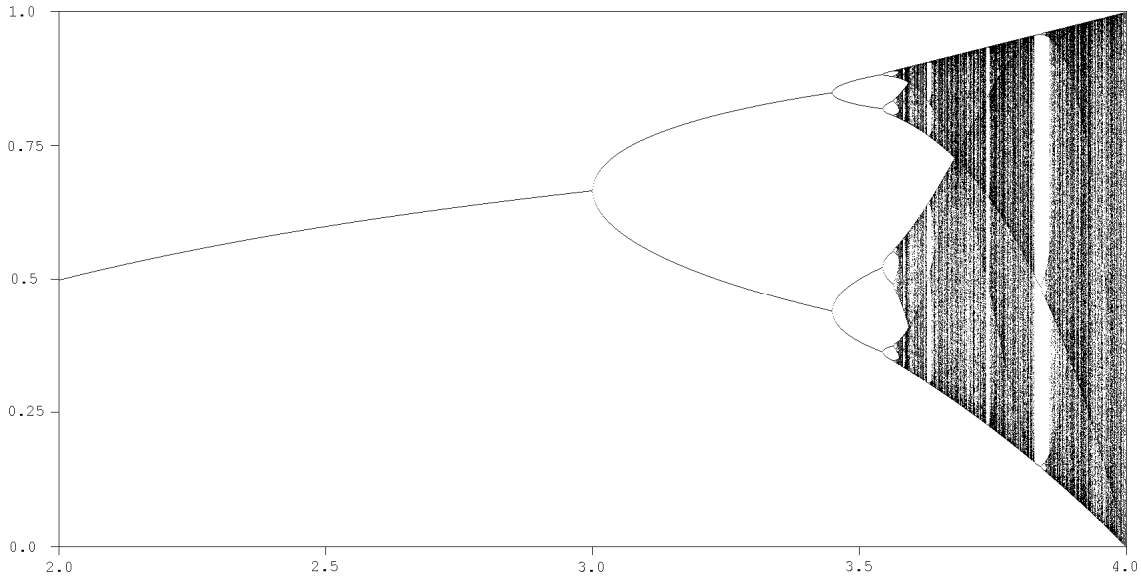

Fig. 4. The bifurcation diagram for the classical logistic function $\lambda x(1-x)$.

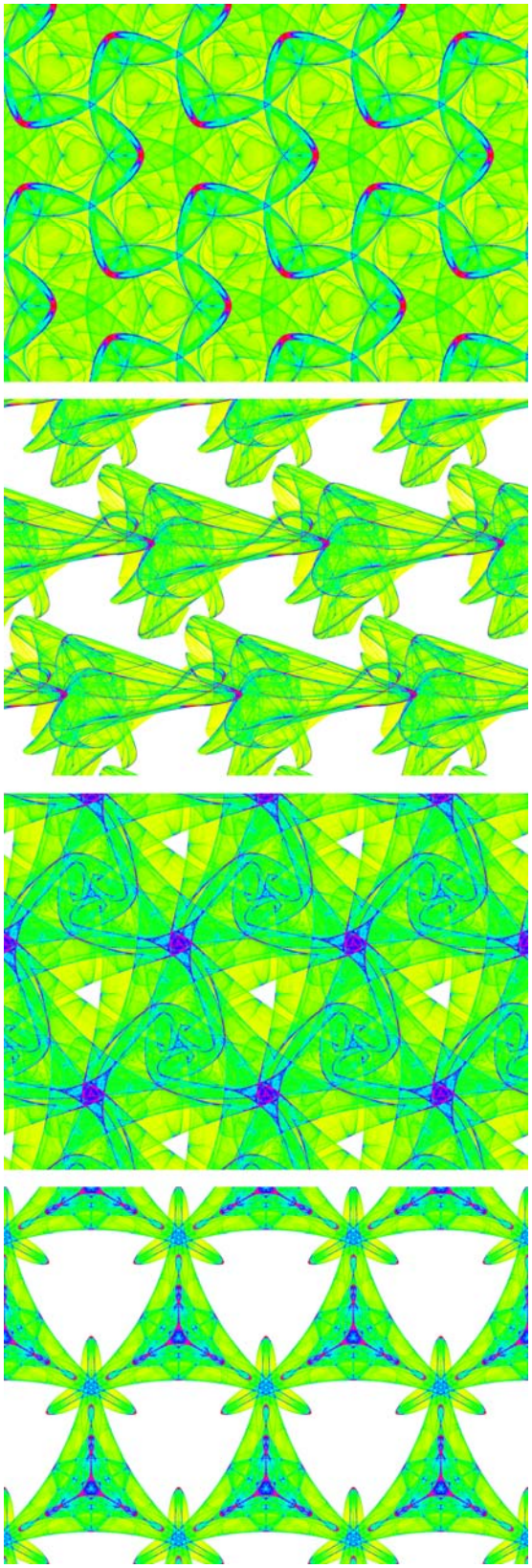

Fig. 5. A family of chaotic attractors evolving from *p31m* to *p3* to *p3m1* crystallographic symmetry.